scientific reports

Check for updates

OPEN

Metals (Ga, In) decorated fullerenes as nanosensors for the adsorption of 2,2-dichlorovinyldimethyl phosphate agrochemical based pollutant

Michael A. Akpe[1,2], Gideon A. Okon[1,3], Hitler Louis[1,2]✉, Innocent Benjamin[1]✉, Martilda U. Akem[1,2], Onyebuenyi I. Brown[1,2], Stephen A. Adalikwu[1] & Adedapo S. Adeyinka[4]

Owing to the fact that the use of 2,2-dichlorovinyldimethylphosphate (DDVP) as an agrochemical has become a matter of concern due to its persistence and potential harm to the environment and human health. Detecting and addressing DDVP contamination is crucial to protect human health and mitigate ecological impacts. Hence, this study focuses on harnessing the properties of fullerene (C60) carbon materials, known for their biological activities and high importance, to develop an efficient sensor for DDVP. Additionally, the sensor's performance is enhanced by doping it with gallium (Ga) and indium (In) metals to investigate the sensing and trapping capabilities of DDVP molecules. The detection of DDVP is carefully examined using first-principles density functional theory (DFT) at the Def2svp/B3LYP-GD3(BJ) level of theory, specifically analyzing the adsorption of DDVP at the chlorine (Cl) and oxygen (O) sites. The adsorption energies at the Cl site were determined as − 57.894 kJ/mol, − 78.107 kJ/mol, and − 99.901 kJ/mol for Cl_DDVP@C60, Cl_DDVP@Ga@C60, and Cl_DDVP@In@C60 interactions, respectively. At the O site, the adsorption energies were found to be − 54.400 kJ/mol, − 114.060 kJ/mol, and − 114.056 kJ/mol for O_DDVP@C60, O_DDVP@Ga@C60, and O_DDVP@In@C60, respectively. The adsorption energy analysis highlights the chemisorption strength between the surfaces and the DDVP molecule at the Cl and O sites of adsorption, indicating that the O adsorption site exhibits higher adsorption energy, which is more favorable according to the thermodynamics analysis. Thermodynamic parameters (ΔH and ΔG) obtained from this adsorption site suggest considerable stability and indicate a spontaneous reaction in the order O_DDVP@Ga@C60 > O_DDVP@In@C60 > O_DDVP@C60. These findings demonstrate that the metal-decorated surfaces adsorbed on the oxygen (O) site of the biomolecule offer high sensitivity for detecting the organophosphate molecule DDVP.

The abuse or misuse of agrochemicals leads to serious environmental problems and hazardous conditions especially in developing countries where there exists weak or no control laws. The pollution of the environment with agrochemicals is a global problem of concern to the international community. Hampered by the destructive activity of crops pests and diseases, the agricultural sector has devised several means of curbing the unwanted losses caused by plants diseases and crop pests and one of such measures is the application of pesticides. Agrochemicals of the organophosphate (OP) class are widely used as insecticides to control insect pests. Dichlorvos ((2,2-dichlorovinyldimethylphosphate), DDVP); a representative organophosphorus pesticide[1], which has been commonly used in developing countries and many other regions for more than 40 years[2] due to its significant advantages in controlling internal and external parasites in crops and livestock, and its ability to eliminate several pests in houses and farmlands[1,3]. Traded under names such as DDVP, Sniper, Nogos, Dedevap, Nuvan,

[1]Computational and Bio-Simulation Research Group, University of Calabar, Calabar, Nigeria. [2]Department of Pure and Applied Chemistry, University of Calabar, Calabar, Nigeria. [3]Department of Chemical Sciences, Clifford University, Owerrinta, Nigeria. [4]Department of Chemical Sciences, Research Centre for Synthesis and Catalysis, University of Johannesburg, Johannesburg 2006, South Africa. ✉email: louismuzong@gmail.com; benjamininnocent53@gmail.com

Phosvit, Daksh and Vapona[4], DDVP is classified by the World Health Organization (WHO)[5] and United States Environmental Protection Agency (USEPA)[6] as class 2B: possible carcinogens and Class I pollutant (highly toxic) respectively. DDVP has a high vapor pressure of 1.2×10^{-2} mmHg at 20 °C, and density of 1.415 g/mL at 25 °C, it is very soluble in water and possesses the ability to remain in solution and does not easily sorb into sediment[7]. When in solution, DDVP becomes susceptible to both biological and abiotic degradation, though the predominant mechanism is hydrolysis. DDVP is hydrolyzed into dichloroethanol, dichloroacetaldehyde, dichloroacetic acid, dimethyl phosphate and dimethyl phosphoric acid[8]. Its high vapor pressure makes it very volatile, hence inhalation is the major exposure pathway of acute toxicity.

DDVP is reported to be toxic even in low concentrations and there are several reports about the hazardous effects of DDVP on the human body indicating that a higher concentration of DDVP can cause death[9]. It may cause mild skin irritation, allergic skin reaction and damage to the nervous system through prolonged or repeated exposure which is reflected by cholinesterase inhibition[10]. When swallowed the effect is very fatal. Children exposed to DDVP face an increased risk of diabetes and this may lead to the increasing risk of breast cancer in adulthood[11]. Scientific research has demonstrated certain effects of chronic exposure to DDVP on mouse. Those animals exposed to DDVP showed nigrostriatal neuron degeneration and remarkable behavioral impairment. Such animals have representative symptoms called catalepsy which is similar to those of Parkinson's disease in humans[12,13]. Exposure to this substance is inevitable for people in those countries, and with the reports of health risks and damages to humans and other organisms coming from the misuse or abuse of this substance, there is therefore an urgent need to devise more efficient means of removing DDVP residues in the environment and in order to protect people from further physiological damage.

Buckminster fullerene or Bucky ball otherwise called fullerene C_{60} is one of the most commonly studied nanomaterials in the areas of engineering, biomedicine and material science[14]. This is due to its unique spherical structure and physicochemical properties. Literature reports show that C_{60} is very useful in the areas of energy and hydrogen storage, drug delivery, plasmonics, optoelectronics, corrosion prevention; gas, photo-electrochemical and optical sensors[15–20]. Furthermore, C_{60} possesses electron-acceptor- donor properties, sensitivity, extremely large surface area, optical, non-linear, electron and adsorption properties and these properties have over time been enhanced through such methods as chemical functionalization and doping/decoration with hetero atoms[21,22]. As reported by Sadeghi et al.[23] in their work where dichlorosilane (DS) gas was detected with C_{60} fullerene, the adsorption and sensing performance of C_{60} fullerene well improved from − 21.4 to − 84.4, − 86.7 and − 90.7 kJ/mol, simply due to doping with Al, Ga and Zn atoms respectively. Also, Abraham[24], reported that the doping of C_{60} fullerene with Fe and Mn atoms increased the sensitivity to cyanogen halides against pristine C_{60} fullerene. Muz et al.[25], Parlak et al.[26] and Muz[27] in their separate works reported enhanced performance of C_{60} fullerene when doped with B, Al Ga; Si; Mg, Ca, Fe and Zn for the detection and adsorption of 1,3,4-oxadiazole, molnupiravir drug and flouroquinoline antibiotic respectively. It is worthy that agrochemical-based pollutants pose significant complications, including soil, water, and air contamination, loss of biodiversity, and potential harm to humans and wildlife through the food chain[28–30]. These pollutants contribute to health risks, pesticide resistance, and ecological imbalances. Improper use and disposal also contaminate groundwater, affecting drinking water and irrigation[31,32]. Urgent adoption of sustainable agricultural practices and safer alternatives is crucial to safeguard the environment and human health[33].

This study explores the novelty of using pristine-based metals (Ga, In) decorated materials for trapping 2,2-dichlorovinyldimethylphosphate (DDVP), an agrochemical-based pollutant, within the density functional theory (DFT) framework, shedding light on their potential in addressing DDVP contamination. However, there are limitations to consider. While the study provides valuable insights into the adsorption energies and bonding nature between the surfaces and DDVP, further experimental validation is necessary to confirm the theoretical findings. Moreover, the study focuses solely on the chlorine and oxygen adsorption sites; thus, future works should investigate other potential adsorption sites and explore the dynamics of the trapping process. Additionally, examining the stability and reusability of the materials, as well as their performance under various environmental conditions, is crucial. Further research can explore their potential applications in real-world scenarios, such as developing practical sensors and remediation strategies for DDVP pollution. In this comprehensive investigation, we perform frontier molecular orbital analysis to assess the conductivity and reactivity of the surfaces, utilizing natural bond orbital (NBO) analysis to examine charge transfer. Elucidating the bonding nature between the adsorbate and surface is accomplished using the quantum theory of atoms in molecule (QTAIM), while stability of the bonds is determined through non-covalent interaction (NCI). To evaluate the sensing ability, various sensor mechanisms, comparative adsorption energy analysis, and geometric parameters are employed. The computational details, including geometric optimization and calculations, are provided in the study.

Computational details

Density functional theory and geometric optimization of the fullerene C_{60} decorated with Ga and In, and DDVP surfaces was achieved with the aid of Gaussian 16 and GaussView 6.0.16 packages[34]. The geometry optimization was performed with the Becke three parameter Lee–Yang–Parr exchange-functional (B3LYP) together with Def2svp basis set. The combination of the B3LYP exchange-functional with the Def2svp basis set in our study has significant effects on the investigation of trapping 2,2-dichlorovinyldimethylphosphate (DDVP) agrochemical-based pollutant using pristine-based metals (Ga, In) decorated materials. This combination allows for accurate and reliable first-principles calculations within the density functional theory (DFT) framework, enabling a comprehensive analysis of the trapping efficiency and behavior of DDVP on the decorated materials. It provides insights into the electronic structure, adsorption mechanisms, reactivity, and stability of the system, facilitating a deeper understanding of pollutant trapping and contributing to the development of effective strategies for environmental remediation. Substantially, the absence of imaginary frequency in the hessian matrix is evidence

that the optimized structures are in local minima on their potential energy surfaces. NBO 7.0 program[35] was used to study the intermolecular charge transfer as well as the stability of the surfaces. Electronic properties of the studied systems as well as the quantum chemical descriptors were analyzed using frontier molecular orbital, (FMO). Chemcraft 1.6 software was used to visualize the surface plots of the highest occupied molecular orbital and the lowest unoccupied molecular orbital (HOMO–LUMO) energies of the studied surfaces and complexes. Quantum theory of atoms in molecules (QTAIM) analysis and non-covalent interaction (NCI) was employed to characterize the type of bond/bond strength present between the metal doped cage and DDVP adsorbate molecule using the Multiwfn program[36]. Topology parameters like density of all electrons (ρ) Laplacian of electron density ($\nabla^2\rho$), Hamiltonian kinetic energy (K), Lagrangian kinetic energy (G), and potential energy density (V) according to Bader was analyzed and the 2D plot was obtained from visual molecular dynamics (VMD) software program[37]. The adsorption energy of DDVP on the C_{60} decorated with Ga and In was mathematically calculated using the expression $E_{ads} = E_{DDVP/surface} - (E_{DDVP} + E_{surface})$[38]. Where E_{ads} is the adsorption energy of the DDVP on the surface, $E_{DDVP/surface}$ represents the total energy of the complexes after adsorption, E_{DDVP} and $E_{surface}$ represent the energies of DDVP and the decorated C_{60} surfaces respectively. Sensor mechanism was also employed and calculated in these studies to fully get insight on the adsorption efficacy of fullerene C_{60} nanocage towards efficiently sensing the organophosphate molecule. Also, thermodynamic parameters including Enthalpy and Gibbs free energy was calculated at the same quantum theoretical level of theory above[39]. Quantum global parameters as proposed by koopsman were also employed to study the reactivity of the systems as can be depicted in the mathematical expressions in Eq. (1)–(4) below for chemical hardness (η), global softness (σ), chemical potential (μ) and electrophilicity index (ω) respectively[40].

$$\sigma = \frac{1}{2\eta} = \frac{1}{E_{HOMO} - E_{LUMO}} \tag{1}$$

$$\eta = \frac{E_{HOMO} - E_{LUMO}}{2} \tag{2}$$

$$\mu = \frac{E_{HOMO} + E_{LUMO}}{2} \tag{3}$$

$$\omega = \frac{\mu^2}{2\eta} \tag{4}$$

Results and discussion

Different adsorption configurations of dichlorovos (DDVP). In this present study, density functional theory at the B3LYP functional and def2SVP basis set were employed to study the fullerene, its pristine and metal decorated surfaces on interaction with the chlorovos adsorbate. In order to determine the best and most stable configuration for this study, the organophosphate (DDVP) material was interacted on the surfaces via it's oxygen (O) and chlorine (Cl) sites and was stabilized at the ground state by placing a net charge of 0 (Q = 0 lel) with a singlet multiplicity 1 ($M = 2S_T + 1 = 1$) for the pristine, and a duplet multiplicity of 2 ($M = 2S_T + 2 = 2$) for the Ga and In decorated surfaces and their corresponding interactions with the DDVP molecule respectively. The structural parameters which include the bond labels, bond length (before and after) adsorption was studied for the different interactions herein and results recorded on Table 1. The carbon fullerene material (C_{60}) otherwise known as buckminsterfullerene is made up of 60 carbon atoms in a cage-like fused-ring structure, C_{60} consist of twenty hexagons and twelve pentagons in which a carbon atom is bonded to three carbon neighbors. In this study, using the above level of theory the bond lengths observed for the fullerene surface is ranged from 1.398 to 1.456 Å as can be observed on the table. On introduction of the Ga and In metal impurities, the bond lengths were observed to be 1.398 Å to 1.461 Å and 1.399 Å to 1.459 Å for Ga and In decorated surfaces respectively. During the adsorption process of DDVP on the pristine and metal decorated surfaces, on the chlorine (Cl) site of the organophosphate (DDVP) molecule adsorption, at bond labels of C_{51}–C_{48}, C_{51}–C_{50} and C_{51}–C_{52} the bond lengths observed were 1.456 Å, 1.397 Å and 1.456 Å. For Cl_DDVP@Ga@C_{60}, the bond labels and lengths observed were 1.456 Å at C_{60}–C_{34}, 1.470 Å at C_{60}–C_{35}, 1.475 Å at C_{60}–C_{30} and 2.334 Å for the distance between the doped metal and cage at Ga_{61}–C_{60}. Considering Cl_DDVP@In@C_{60} the bond lengths observed were 1.457 Å at bond label of C_{60}–C_{30}, 1.340 Å noticed at bond label of C_{60}–C_{34}, 1.454 Å seen at C_{60}–C_{35} and metal decoration bond length (after interaction) of 3.446 Å at In_{61}- C_{34}. Meanwhile, at the oxygen (O) adsorption site of the DDVP molecule on the different surfaces, bond lengths of 1.454 Å, 1.456 Å, and 1.455 Å corresponding to bond labels of C_{51}–C_{52}, C_{48}–C_{47}, and C_{52}–C_{53} for O_DDVP@C60 system. For O_DDVP@Ga@C_{60}, the bond lengths were 1.468 Å, 1.472 Å, 1.445 Å and 2.503 Å for bond labels of C_{34}–C_{33}, C_{46}–C_{34}, C_{34}–C_{60} and Ga_{61}–C_{34} while for O_DDVP@In@C60 the bond lengths observed were 1.465 Å, 1.434 Å, 1.463 Å and 2.752 Å for C_{34}–C_{46}, C_{34}–C_{69}, C_{34}–C_{33} and In_{61}–C_{34} respectively. The bond lengths of compounds give useful insights on the reactivity, phase of matter, polarity, and biological interaction processes[41]. According to[42], existence of short bond length in a biomolecule result in stronger bonding energy between the interacting atoms because the short distance provides room for an overlap of electron cloud between atomic nuclei which results in strong electrostatic attraction between them. Again, according to Louis et al.[43], short bond length entails reactivity of the interacting molecule and suggest that the atoms may not be strongly reactive with an interacting specie. Conversely, the reverse may hold for compounds with longer bond length. In this study, as depicted in Figs. 1 and 2 the structural analysis

Systems	Bond lengths (Å)		
	Bond label	Before ads	After ads
Cl_DDVP@C_{60}	C51–C48	1.456	1.456
	C51–C50	1.398	1.397
	C51–C52	1.456	1.456
Cl_DDVP@Ga@C_{60}	C60–C34	1.452	1.456
	C60–C35	1.461	1.47
	C60–C30	1.461	1.475
	Ga61–C60	2.448	2.334
Cl_DDVP@In@C_{60}	C60–C30	1.459	1.457
	C60–C34	1.446	1.34
	C60–C35	1.459	1.454
	In61–C34	2.679	3.446
O_DDVP@C_{60}	C51–C52	1.456	1.454
	C48–C47	1.456	1.456
	C52–C53	1.456	1.455
O_DDVP@Ga@C_{60}	C34–C33	1.461	1.468
	C46–C34	1.461	1.472
	C34–C60	1.452	1.445
	Ga61–C34	2.448	2.503
O_DDVP@In@C_{60}	C34 –C46	1.459	1.465
	C34–C60	1.446	1.434
	C34–C33	1.459	1.463
	In61–C34	2.679	2.752

Table 1. Tabular presentation of the bond lengths (Å) before and after adsorption calculated at the DFT/B3LYP-GD3BJ/def2svp level of theory.

shows that there was considerable increase for most of the systems after interaction in both absorption site of studies. This result suggests the reactivity of the atoms towards adsorbing the DDVP molecule for the effective control of household pests and other insects especially the doped fullerene surfaces.

Reactivity and stability descriptors. Frontier molecular orbital (FMO) illustrate the electron donor–acceptor interacting systems using the highest occupied molecular orbital (HOMO) and lowest unoccupied molecular orbital (LUMO) of electrons in the molecule. HOMO is an electron donating orbital while the LUMO is the electron accepting orbital[44–46]. The energy difference between the two terms (HOMO and LUMO) is called the energy gap. HOMO–LUMO are collectively referred to as the frontier molecular orbitals because they lie at the outermost boundaries of chemical specie. More chemical reactivity and simpler electron evolutions from the HOMO to the LUMO are accompanied with a smaller energy gap. A larger energy gap indicates more chemical stability, which influences how easily electrons may be transported from HOMO to LUMO[47–50]. The HOMO–LUMO energy gap of a system can be calculated applying the Eq. (5) while the HOMO–LUMO visualized plots are shown on Fig. 3.

$$\Delta E = E_{HOMO} - E_{LUMO} \tag{5}$$

In this study, the energy gap of DDVP in its pure form is 6.395 eV. while $C_{60,}$ Ga@$C_{60,}$ and In@C_{60} has energy gap of 3.75 eV, 1.387 eV, and 1.225 eV respectively. However, when doped with Gallium(Ga) and Indium(In), the fluctuation in the energy gap observed in Table 2 shows a reduction in most of the complexes and an increase in some of the complexes such as; Cl_DDVP@In@C_{60} with energy gap Eg(eV) of 1.225 eV as compare to when it is in it pure state/surface with energy gap of 2.612 eV which justifies the fact that the smaller the energy gap the more reactive the molecule and the faster the electron movement will occur. when DDVP is interacted with chlorine (Cl), at Cl_DDVP@Ga@C_{60}, it exhibits energy gap of 3.265 eV which shows a fall/decrease in the energy gap as compared to when it was a pure Ga surface with energy gap of 3.429 eV, there is a slight decrease in the energy gap as the result of the influence of the doped properties. However, when the organophosphate biomolecule was doped with Cl at (Cl_DDVP@In@C_{60}), the energy gap slightly increases as compare to In@C_{60} with energy gap of 1.225 eV, the increase in energy gap make it less reactive. Likewise, interacting DDVP with oxygen (O), which also shows a shift in the energy gap from 2.721 eV, 1.252 eV, 2.612 eV, to 1.333 eV, 1.116 eV, 0.489 eV respectively. Thus, interacting DDVP with oxygen (O), as follows O_DDVP@$C_{60,}$ O_DDVP@In@$C_{60,}$ and O_DDVP@Ga@$C_{60,}$ influences a huge decrease in the energy gap and thereby reveal their aptness for use to detect DDVP biomolecule.

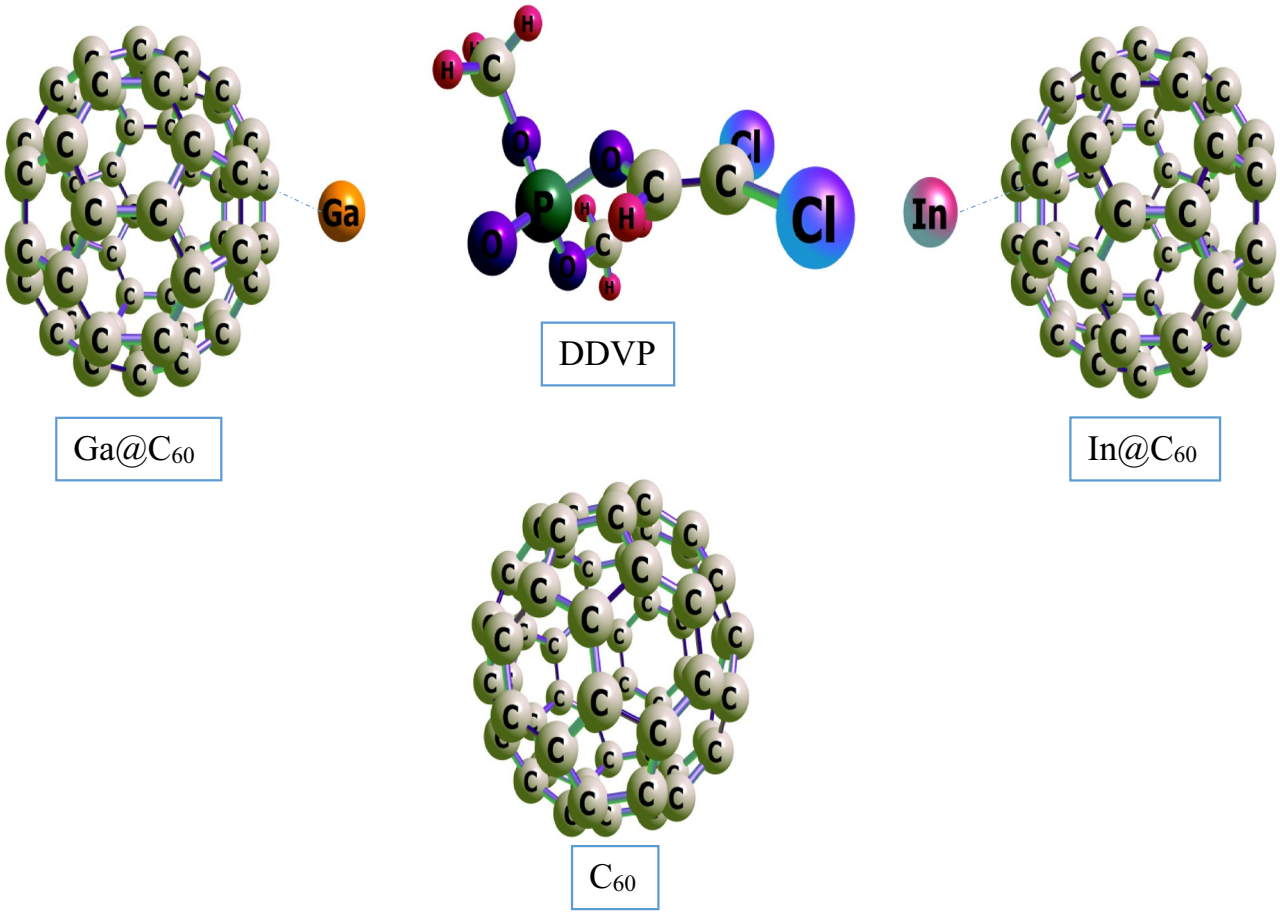

Figure 1. Optimized structures of the DDVP molecule, the fullerene nanocage, and its Ga and In metal doped surfaces.

In investigating the electronic properties of the absorbent molecule after the absorption of the organophosphate (DDVP) biomolecule, DFT calculation were employed in order to have full grasp of the reactivity, conductivity and stability of the materials in these studies which are significant properties for a sensor or drug delivery system[51,52]. Here, the difference between the HOMO–LUMO energy gap which is often expressed as energy gap is considered as very important factor for measuring the conducting potential of an electrochemical sensor material. Increase in the conductivity produces a detected electrochemical signal from which the absorption process can be confirmed, and the DDVP molecule can be detected. The chemical global hardness (η) value indicates higher chemical stability for the structure with a reduced chemical reactivity, The chemical softness (σ) has an inversely proportional relationship with the hardness, an increase in the σ indicates an increase in the chemical reactivity with the reduced chemical stability of the structure, The chemical potential (μ) can be used to determine the stability of the investigated structure to determine the direction of electron transfer from the absorbate to absorbent, The electrophilicity index (ω) also indicates an increase in the chemical reactivity while the electronegativity (χ) can be applied to determine the direction of the flow of electron in a chemical system where the electrons move towards the higher electronegative region from a lower one[53,54]. Applying the mathematical formulas has shown in Eq. (1)–(4) of the computational details section for chemical hardness (η), global softness (σ), chemical potential (μ) and electrophilicity index (ω) based on the Koopmans's theorem.

Density of state (DOS) analysis. The density of states (DOS) is a reactivity parameter that helps us gain insight on the molecular orbital contributions of the participating atoms present in an interacting molecule. In this current research, the participating atom fragments within the pristine fullerene and its Ga and In metal doped surfaces on interacting with the biomolecule (dichlorovos) on its chlorine (Cl) and Oxygen (O) site were studied at the same level of computational theory. The density of state is observed to be continuous. The total density of states (TDOS), the partial density of state (PDOS) and the overlap density of state (OPDOS) were fully employed to determine the reactivity and contributions of each atom fragments from the HOMO to the LUMO molecular orbital as well as the tracking of band gap changes by utilizing the fermi energy level which is indicated by a dotted line on the plot[55]. The fermi energy level demarcates the TDOS and PDOS which are on the left axis from the OPDOS which is on the right side of the plot. From the different plots of the interactions as depicted on Fig. 4 between the C_{60} fullerene doped with metals interacted with DDVP molecule which was made possible by employing the Multifwn software for the fragments generation and Origin software[51] for the maps respectively, the plots clearly show that in the interactions involving the pristine cage and DDVP on both sites

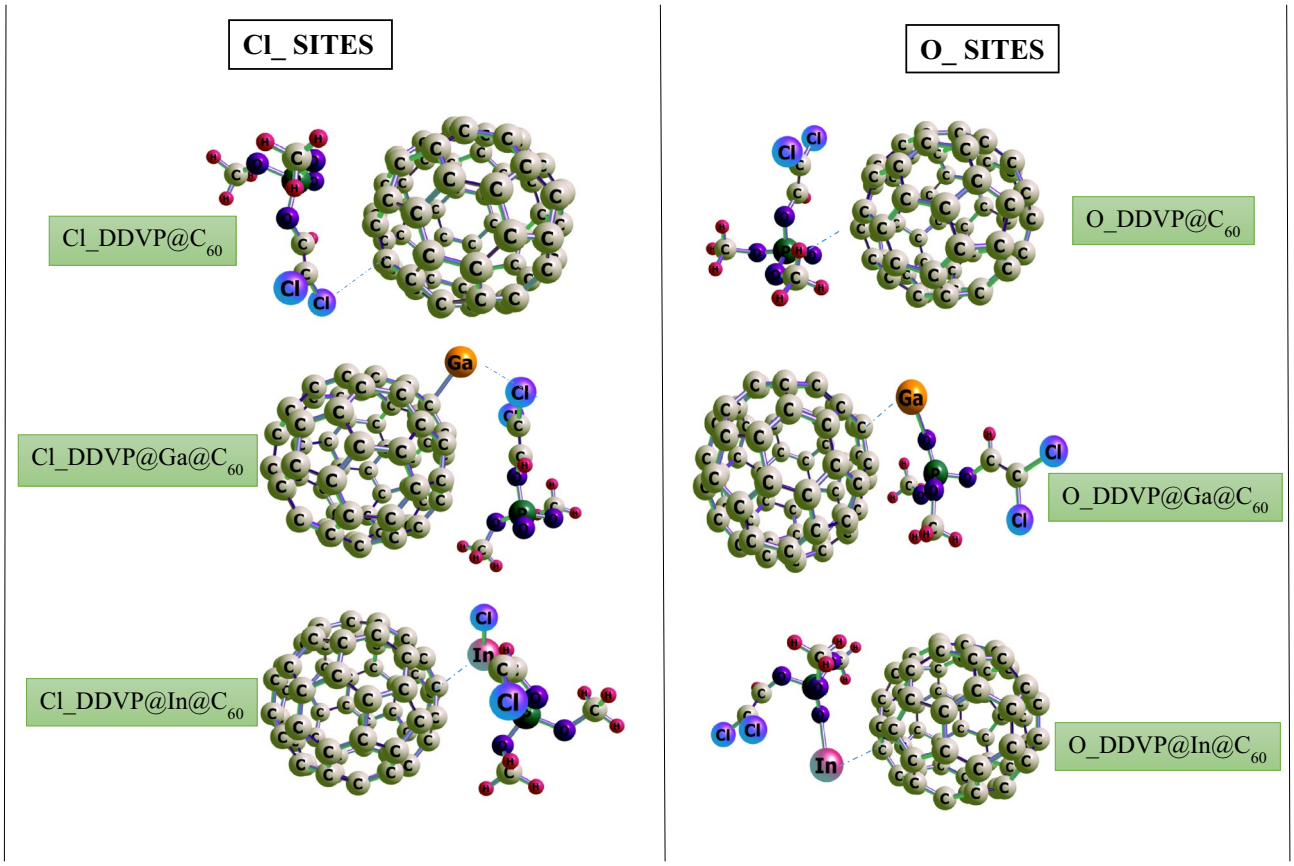

Figure 2. Optimized structures of the fullerene nanocage and its Ga and In metal doped surfaces interacting with the DDVP molecule at the Cl and O adsorption site.

of adsorption, oxygen (O) fragments were the most contributive fragments at the fermi energy level of − 6.91 eV and − 6.89 eV for Cl_DDVP@C_{60} and O_DDVP@C_{60} respectively. On plots labelled Cl_DDVP@Ga@C_{60}, and Cl_DDVP@In@C_{60} the most dominant atom fragment from the HOMO to the LUMO molecular orbital were Ga and In atoms respectively at fermi energy level of − 6.75 eV and − 6.12 eV respectively. Also, on the O site of adsorption of the biomolecule, the major contributions were observed in Ga and In atoms respectively at energy level of about − 5.89 eV corresponding to O_DDVP@Ga@C_{60} and O_DDVP@In@C_{60} respectively. The result observed herein for the density of state clearly shows the importance and enhancement brought about by the metal dopants, as we can clearly see their high contributions and dominance in the interactions, as the different maps replicates the exact number of molecular orbitals present at different quantum state at a certain unit of energy interval.

Natural bond orbital (NBO) analysis. Natural bond orbital (NBO) analysis is a method used for inspecting the chemical features of a given composite in terms of bonding, antibonding (donor–acceptor) and delocalization interactions. This includes other properties like intra and intermolecular charge transfer, stability, and reactivity of bonds between donor and acceptor orbitals. The NBO output file has donor, acceptor and neutral orbital type as the primary source to transform wave function optimally into localized lone pairs[56,57]. The interaction between acceptor non-Lewis NBOs and the donor Lewis type NBOs are examined and estimated through the second order perturbation theory. The electron distribution densities in atoms are determined using the natural bond orbital analysis in computational methods. For NBO (i) and acceptor NBO (j), the stabilization energy $E^{(2)}$ with delocalization is extracted using Eq. (6)[58,59].

$$E^{(2)} = \Delta E_{ij} = -qi\ F^2_{(ij)}/E_i - E_j \tag{6}$$

where qi denotes the electron donor orbital occupancy, Ei and Ej stands for the orbital energies of the donor and acceptor orbitals. Before the interactions (surfaces), it was observed that Ga@C_{60} has the highest stabilization of 64.79 kcal/mol and 11.67, 29.33 kcal/mol from the σ O_5–P_8 → π*O_4–P_8 and σ O7–P_8 → π*O_4–P_8 and πC30–C31–π * C34–C60 → π * C34–C46—π * C45–C55 donor–acceptor orbital. While, C_{60} and In@C_{60} are seen to have the minimum stabilization energy of 14.23 and 14.22 kcal/mol, 11.67 and 29.22 kcal/mol from π C43–C44–π * C 45–C55 → πC50–C51–π * C36–C49 and πC30–C31–π * C34–C60 → π * C34–C46–π * C45–C55 from the donor to acceptor orbitals respectively. After the interactions (complex), Cl_DDVP@C_{60} and Cl_DDVP@In@C_{60} with stabilization energy of 15.25, 14.71 kcal/mol, 3.96 and 9.85 kcal/mol from πC7–C19_π * C21—C22 → π

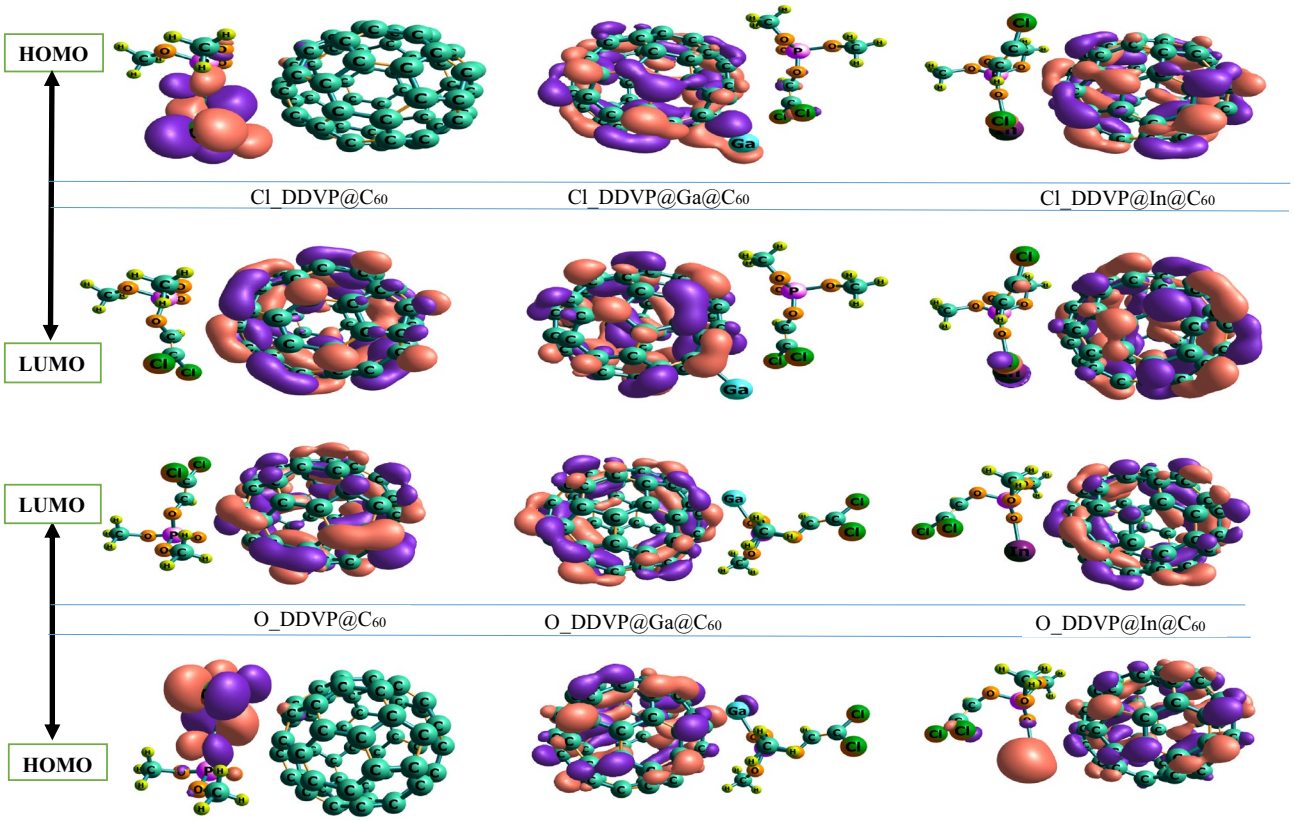

Figure 3. 3-Dimensional Maps of the HOMO/LUMO electrons visualized distributions of the complexes on both sites (Cl and O) of adsorption done by employing the Chemcraft software.

Systems	HOMO (a.u)	LUMO (a.u)	IP (eV)	EA (eV)	μ (eV)	η (eV)	Eg (eV)	σ/eV	ω	x (eV)
C_{60}	−0.232	−0.370	6.313	10.068	−8.19	1.878	3.755	0.532	62.980	8.190
DDVP	−0.247	−0.012	6.721	0.327	−3.52	3.197	6.395	0.310	19.852	3.523
$Ga@C_{60}$	−0.177	−0.126	4.816	3.429	−4.12	0.694	1.387	1.441	5.896	4.123
$In@C_{60}$	−0.168	−0.123	4.572	3.347	−3.96	0.612	1.225	1.633	4.799	3.959
$Cl\_DDVP@C_{60}$	−0.227	−0.127	6.177	3.456	−4.82	1.361	2.721	0.735	15.781	4.816
$Cl\_DDVP@Ga@C_{60}$	−0.166	−0.120	4.517	3.265	−3.89	0.626	1.252	1.598	4.738	3.891
$Cl\_DDVP@In@C_{60}$	−0.225	−0.129	6.123	3.510	−4.82	1.306	2.612	0.766	15.149	4.816
$O\_DDVP@C_{60}$	−0.227	−0.178	6.177	4.844	−5.51	0.667	1.333	1.500	10.121	5.510
$O\_DDVP@Ga@C_{60}$	−0.133	−0.115	3.619	3.129	−3.37	0.245	0.489	4.083	1.394	3.374
$O\_DDVP@In@C_{60}$	−0.141	−0.111	3.837	2.721	−3.28	0.558	1.116	1.793	2.999	3.279

Table 2. Analysis of the global quantum descriptors, Ionization Potential (IP, eV), Electron Affinity (EA, eV), Chemical Potential (μ, eV), Global Hardness (η, eV), Global Softness (S, eV^{-1}), and Electrophilic Index (ω, eV) calculated for all systems estimated using the B3LYP-GD3BJ/def2svp level of theory.

C_9—C_{10}—π* C_{11}–C_{59} and LP C_{60}–LP*$_{(2)}In_{61}$ → π C_{34}–C_{46}–LP*$_{(2)}In_{61}$ donor to acceptor orbitals. However, O_DDVP@C_{60} and O_DDVP@Ga@C_{60} exhibit stabilization energy of 7.63, 5.12 and 30.15,4.86 kcal/mol from πC_{63}–H_{75}–σ* C_{76}–C_{178} → σO_{65}–P_{68}–σ* O_{66}–P68 and LP C_{60}–LP* Ga61 → σC_{34}–C_{46}–LP* Ga61 donor to acceptor orbitals. Likewise, O_DDVP@In@C_{60} with minimal stabilization energy of 3.96 and 9.85 kcal/mol from πC34–C46–LP* In61 → LP C60–LP* In61 donor to acceptor orbital respectively. It was observed that the adsorption of DDVP on the doped surfaces brought about a decreased in the perturbation energy of the system including increased in the conductivity of the systems as recorded in Table 3.

Topological analysis. *Quantum theory of atoms in molecules.* The quantum theory of atoms in molecules (QTAIM) as a topological study tool is very useful and important in that it offers important details on molecular and atomic interactions of bonds, particularly that of hydrogen bonds, hence it is the easiest form of interaction[60,61]. QTAIM shows the molecular and reduced nature of the electronic structures of atoms[62]. The

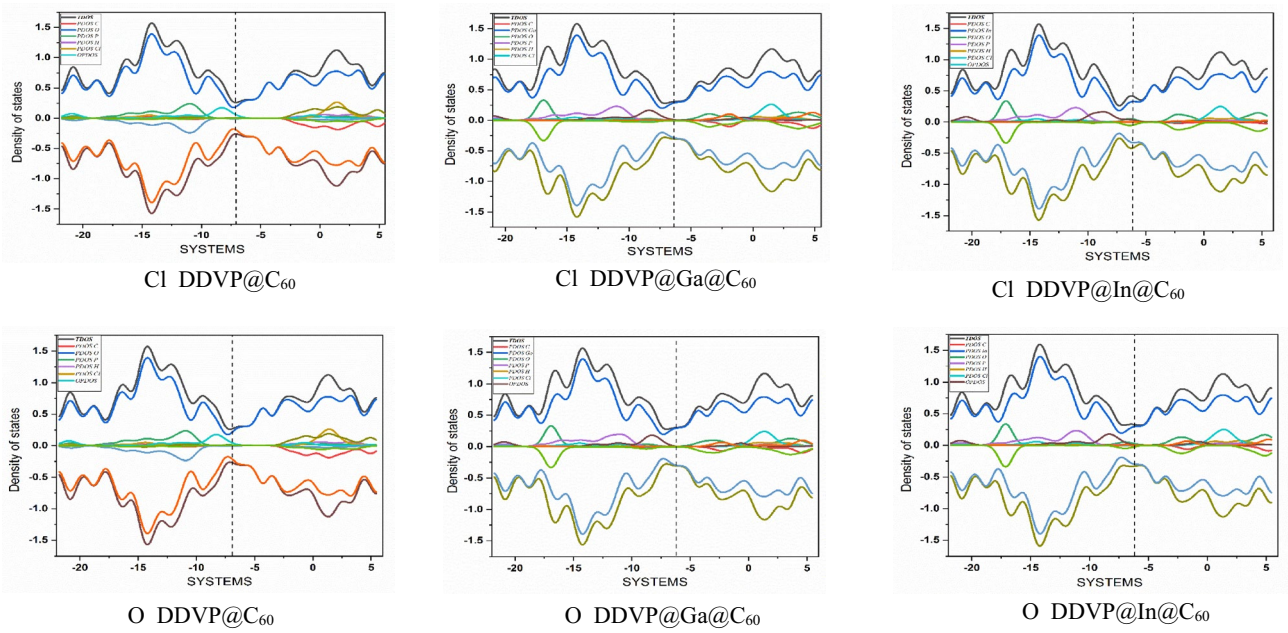

Figure 4. Density of State plots of the adsorbed organophosphate molecule (DDVP) on the pristine and metal doped fullerene surfaces on both Cl and O adsorption sites done using the Origin software.

Donor	Donor (i)	Acceptor (j)	E^2 Kcal/mol	E(j)–E(i)	F(i, j)
C_{60}	π C_{43}–C_{44}	π* C_{45}–C_{55}	14.23	0.32	0.060
	π C_{50}–C_{51}	π* C_{36}–C_{49}	14.22	0.32	0.060
DDVP	σ O5–P8	π* O4–P8	64.79	0.96	0.224
	σ O7–P8	π* O4–P8	82.35	0.97	0.253
Ga@C_{60}	π C_{30}–C_{31}	π* C_{34}–C_{60}	11.67	0.28	0.074
	π* C_{34}–C_{46}	π* C_{45}–C_{55}	29.33	0.08	0.079
In@C_{60}	π C_{21}–C_{22}	π* C_7–C_{19}	7.37	0.32	0.061
	π C_{29}–C58	π* C_{11}–C_{59}	6.76	0.31	0.059
Cl_Chloro@C_{60}	π C7–C19	π* C_{21}–C_{22}	15.25	0.31	0.061
	π C9–C10	π* C_{11}–C_{59}	14.71	0.31	0.060
Cl_Chloro@In@C_{60}	LPC60	LP*(2)In61	9.85	0.06	0.035
	π C34–C46	LP*(2)In61	3.96	0.18	0.034
O_Chloro@C_{60}	π C63–H75	σ* C_{76}–Cl_{78}	7.63	0.69	0.065
	σ O 65–P68	σ* O66–P68	5.12	0.99	0.066
O_Chloro@Ga@C_{60}	LPC 60	LP* Ga61	30.15	0.10	0.044
	σ C 34–C 46	LP* Ga61	4.86	0.21	0.041
O_Chloro@In@C_{60}	π C 34–C 46	LP* In61	3.96	0.18	0.034
	LP C 60	LP* In61	9.85	0.06	0.035

Table 3. Natural bond orbital analysis of the various interactions, showing their second order perturbation energy at the Cl and O site of adsorption.

commencement of atoms in molecules AIM, explains the hydrogen bonding and its perfect knowledge. According to studies on atoms in molecules (AIM), the presence of synthetic bonds between homoatoms or heteroatoms is defined by the presence of bond critical points. These instinctive possessions involve several charge densities and Laplancians of the charge density. In this study we have carefully made optimum use of the QTAIM theory in agreement with the idea of Bader[63], to anatomize the various features of the intermolecular hydrogen bond critical points in the studied system (DDVP). In QTAIM analysis, it is required to distinguish the following parameters the density of all electrons ρ(r), Laplacian of electron density $\nabla^2(r)$, Lagrangian kinetic energy G(r), Hamiltonian kinetic energy K(r), potential electron energy density V(r), total electron energy density H(r), electron localization function (ELF), Eigen values (λ_1, λ_2, λ_3) of hessian[64,65]. The Laplacian electron density $\nabla^2(r)$ and total electron energy density H(r) show the covalent interactions and their nature. The positive values of $\nabla^2(r)$ and negative values of H(r) show an average interaction (slightly covalent) while the negative values for $\nabla^2(r)$

and H(r) indicate a strong covalent interaction. The bond elliphilicity (ε) aids in determining the stability of the interactions in relation to the Eigenvalues (λ_1, λ_2, λ_3) of the Hessian matrix. Elliphilicity values less than 1 depict stability in the structure of the interactions while values greater than 1 show instability in the structure of the interactions. The electron localization function (ELF) helps in understanding the experimental idea of electron localization. It is a powerful tool that explains extensively the character of the electrons in a system which includes bonding situations in a system. Higher values (between 0.5 and 1 a.u.) of ELF obviously indicate strongly localized and electron localized function while lower values (less than 0.5) of ELF indicate strongly delocalized function. From Table 4, it is seen that there is high delocalization of electrons[56–58].

However, literature assessments have shown that the strength of an interaction can be estimated using the density of all electrons such that a higher ρ(r) value from ρ > 0.1 a.u tells a strong existence of strong covalent interaction while a lesser value of ρ(r) shows a weak non-covalent interaction[66], for all the interactions Cl_DDVP@C_{60}, Cl_DDVP@Ga@C_{60}, Cl_DDVP@In@C_{60}, and O_DDVP@C_{60}, O_DDVP@Ga@C_{60}, O_DDVP@In@C_{60}, there exist a weak non-covalent interaction within the complexes. Therefore, when $\nabla^2\rho(r) > 0$ and H(r) > 0) it implies that the interaction is non-covalent while $\nabla^2\rho(r) > 0$ and H(r) < 0 it shows a partial covalent interaction. While,$\nabla^2\rho(r) < 0$ and H(r) < 0, depicts a covalent interaction between the adsorbent and adsorbate. It can be seen from the QTAIM table above that the bond existing between DDVP (organophosphate molecule) and doped C_{60} is a

Complexes	CP	Bond	ρ(r)	G(r)	K(r)	V(r)	H(r)	∇2ρ*	ELF	λ1	λ2	λ3
Cl_DDVP@C_{60}	C_{117}–C_{51}	233	0.0084	0.0049	−0.0057	−0.0043	0.0005	0.0219	0.0401	0.0307	−0.0043	−0.0045
	C_{178}–C_{48}	203	0.0061	0.0040	−0.0005	−0.0034	0.0005	0.0182	0.0211	0.0213	−0.0025	−0.0005
	C_{76}–C_{48}	209	0.0063	0.0046	−0.0004	−0.0042	0.0004	0.0203	0.0177	0.0228	−0.0018	−0.0007
	O_{67}–C_{54}	130	0.0057	0.0054	−0.0014	−0.0040	0.0014	0.0274	0.0094	0.0314	−0.0002	−0.0037
	C_{61}–C_{46}	116	0.0056	0.0039	−0.0004	−0.0034	0.0004	0.0176	0.0169	0.0216	−0.0008	−0.0030
	C_{63}–C_{53}	184	0.0084	0.0049	−0.0001	−0.0047	0.0001	0.0206	0.0386	0.0282	−0.0044	−0.0030
	O_{64}–C_{54}	151	0.0059	0.0048	−0.0012	−0.0036	0.0012	0.0243	0.0129	0.0308	−0.0023	−0.0040
Cl_DDVP@Ga@C_{60}	O_{67}–C_{49}	131	0.0066	0.0058	−0.0014	−0.0043	0.0014	0.0291	0.0130	0.0375	−0.0047	−0.0036
	O_{66}–C_{49}	163	0.0046	0.0044	−0.0013	−0.0031	0.0013	0.0231	0.0068	0.0274	−0.0011	−0.0031
	Ga_{61}–C_{60}	234	0.0414	0.0281	−0.0008	−0.0273	0.0008	0.0116	0.0204	−0.0354	0.0188	−0.0374
	C_{77}–C_{35}	193	0.0102	0.0065	−0.0001	−0.0063	0.0001	0.0269	0.0426	0.0344	−0.0030	−0.0044
	C_{179}–Ga_{61}	236	0.0090	0.0035	−0.0000	−0.0035	0.0000	0.0141	0.0915	0.0236	−0.0046	−0.0048
	H_{73}–C_{27}	104	0.0051	0.0035	−0.0007	−0.0028	0.0007	0.0173	0.0148	0.0214	−0.0015	−0.0025
	H_{75}–C_{25}	93	0.0047	0.0033	−0.0007	−0.0026	0.0007	0.0163	0.0131	0.0198	−0.0013	−0.0021
Cl_DDVP@In@C_{60}	C_{178}–C_{43}	144	0.0081	0.0050	−0.0004	−0.0045	0.0004	0.0219	0.0339	0.0285	−0.0014	−0.0051
	In_{61}–C_{34}	109	0.0058	0.0035	−0.0007	−0.0027	0.0007	0.0172	0.0237	0.0227	−0.0019	−0.0035
	C_{176}–C_{60}	147	0.0041	0.0037	−0.0012	−0.0025	0.0012	0.0202	0.0063	0.0242	−0.0011	−0.0028
	O_{68}–C_{37}	182	0.0097	0.0083	−0.0013	−0.0069	0.0013	0.0389	0.0228	0.0499	−0.0081	−0.0029
	C_{179}–H_{72}	236	0.0039	0.0023	−0.0008	−0.0015	0.0008	0.0126	0.0140	−0.0030	−0.0028	0.0185
	C_{64}–C_{35}	185	0.0082	0.0050	−0.0002	−0.0048	0.0002	0.0213	0.0344	0.0032	−0.0023	−0.0045
	C_{179}–C_{49}	234	0.0057	0.0037	−0.0005	−0.0031	0.0005	0.0170	0.0194	0.0198	−0.0018	−0.0010
O_DDVP@C_{60}	O_{64}–C_{51}	129	0.0088	0.0077	−0.0014	−0.0062	0.0014	0.0370	0.0188	0.0465	−0.0032	−0.0062
	C_{63}–C_{51}	165	0.0074	0.0045	−0.0002	−0.0043	0.0002	0.0191	0.0306	0.0250	−0.0042	−0.0016
	H_{72}–C_{50}	122	0.0041	0.0029	−0.0006	−0.0023	0.0006	0.0144	0.0107	0.0172	−0.0023	−0.0004
	C_{178}–C_{49}	186	0.0059	0.0037	−0.0005	−0.0032	0.0005	0.0173	0.0216	0.0217	−0.0025	−0.0018
	C_{177}–C_{36}	212	0.0084	0.0050	−0.0005	−0.0044	0.0005	0.0222	0.0387	0.0299	−0.0047	−0.0029
	H_{74}–C_{52}	87	0.0062	0.0044	−0.0011	−0.0032	0.0011	0.0222	0.0189	0.0296	−0.0051	−0.0022
O_DDVP@Ga@C_{60}	O_{67}–C_{44}	150	0.0076	0.0064	−0.0014	−0.0049	0.0014	0.0314	0.0169	0.0400	−0.0037	−0.0048
	Ga_{61}–C_{34}	223	0.0319	0.0134	0.0024	−0.0158	−0.0024	0.0440	0.3224	0.0915	−0.0240	−0.0234
	H_{71}–C_{43}	111	0.0039	0.0027	−0.0007	−0.0019	0.0007	0.0142	0.0100	0.0177	−0.0024	−0.0010
	C_{62}–C_{41}	124	0.0031	0.0023	−0.0005	−0.0017	0.0005	0.0112	0.0066	0.0129	−0.0003	−0.0013
	O_{68}–C_{33}	166	0.0078	0.0066	−0.0014	−0.0052	0.0014	0.0325	0.0171	0.0418	−0.0061	−0.0031
	C_{63}–C_{45}	172	0.0061	0.0041	−0.0005	−0.0035	0.0005	0.0185	0.0202	0.0231	−0.0031	−0.0014
O_DDVP@In@C_{60}	O_{68}–C_{44}	157	0.0079	0.0067	−0.0014	−0.0052	0.0014	0.0324	0.0179	0.0401	−0.0026	−0.0050
	In_{61}–C_{34}	105	0.0256	0.0138	0.0013	−0.0151	−0.0013	0.0499	0.1762	0.0874	−0.0182	−0.0192
	O_{65}–C_{44}	158	0.0069	0.0054	−0.0013	−0.0041	0.0013	0.0274	0.0168	0.0310	−0.0005	−0.0031
	O_{67}–C_{44}	189	0.0080	0.0067	−0.0014	−0.0053	0.0014	0.0329	0.0186	0.0417	−0.0033	−0.0054
	H_{71}–C_{43}	193	0.0047	0.0031	−0.0007	−0.0024	0.0007	0.0157	0.0140	0.0205	−0.0028	−0.0019

Table 4. Calculated topological parameters obtained at the bond critical point (BCP) of the interactions at the Cl and O sites of adsorption estimated using the Multiwfn software package.

weak non-covalent interaction. Furthermore, the calculated values for $G(r)/|V|(r) > 1$ show non-covalent interaction while $G(r)/|V|(r) < 1$ but greater than 0.5 shows partial covalent interaction and $G(r)/|V|(r) < 0.5$ signifies non—covalent interaction. Thus, $G(r)/|V|(r)$ shows non-covalent interaction. As seen in Table 4, the negative values of K(r) show strong covalency except for O_DDVP@In@C60 interaction with a positive value of K(r). These interactions are indicated with a brown line as shown in Fig. 5.

Non covalent interaction (NCI). The non-covalent interaction (NCI) analysis was analyzed as a topological parameter in these studies in order to study the noncovalent and nonbonding interactions between the adsorbent surfaces and the DDVP adsorbate biomolecule[67]. NCI studies the nature of the intra and intermolecular interactions present in the interactions which could be hydrogen bonding, van der Waal (vdW) or electrostatic or ionic interactions. Using the reduced gradient (RDG) plots of the product of the second Eigen value of Hessian matrix (λ_2) and the electron density (ρ) value[68]. The interactions were visualized and ascertain using the 3D iso -surface plots as well as the 2D reduced density gradient (RDG) scatter plots as can be observed in Fig. 6 for Cl and O adsorption sites respectively. Considering the 2D RDG scatter plots, interactions are observed as spikes such that the configurations hold; for an attractive—hydrogen bonding interaction sign (λ_2) $\rho < 0$ will be obtained, for a repulsive or steric interaction, sign (λ_2) $\rho > 0$ will be obtainable while for a relatively weak van der Waal interaction, sign (λ_2) $\rho \approx 0$ will be obtained[69]. On the other hand, the 3D isosurface plots is also utilized and interpreted based on the color ranges. The presence of blue color represents hydrogen bonding, the green represents weak van der Waal (vdW) interactions while red coloration represents steric repulsive interactions. Meanwhile, the colors are still found on the 2D iso- surface scatter maps and bears the same interpretations. In this study, it can be observed that there exists steric intramolecular interaction within the C_{60} cage for all interactions as depicted by the reddish isosurface maps. On interaction with the DDVP molecule, there was the presence of weak forces of attraction as seen by the green isosurface which were more on the Cl site of adsorption as well as on the bare fullerene interaction with the biomolecule (O_DDVP@C_{60}) on the O adsorption site. Whereas, the weak van der Waal interaction was minimal on the metal doped systems at the O adsorption site complimented by few (small) blue issosurface which further explains their moderate adsorption energy as when compared to the Cl adsorption site whose adsorption was not favorable due to weak forces of interaction present in them.

Sensor mechanisms. The band gap of a semiconductor material is crucial to understanding the conductivity of the biosensor material. In solid state physics, large band gap between the conduction and valence band of a conducting material with radiation of appropriate wavelength can cause promotion and photoconductivity, a small change in the Energy gap values at a given temperature, exponentially affects electrical conductivity which in turn produces electrical signal and can be related using Eq. (7).

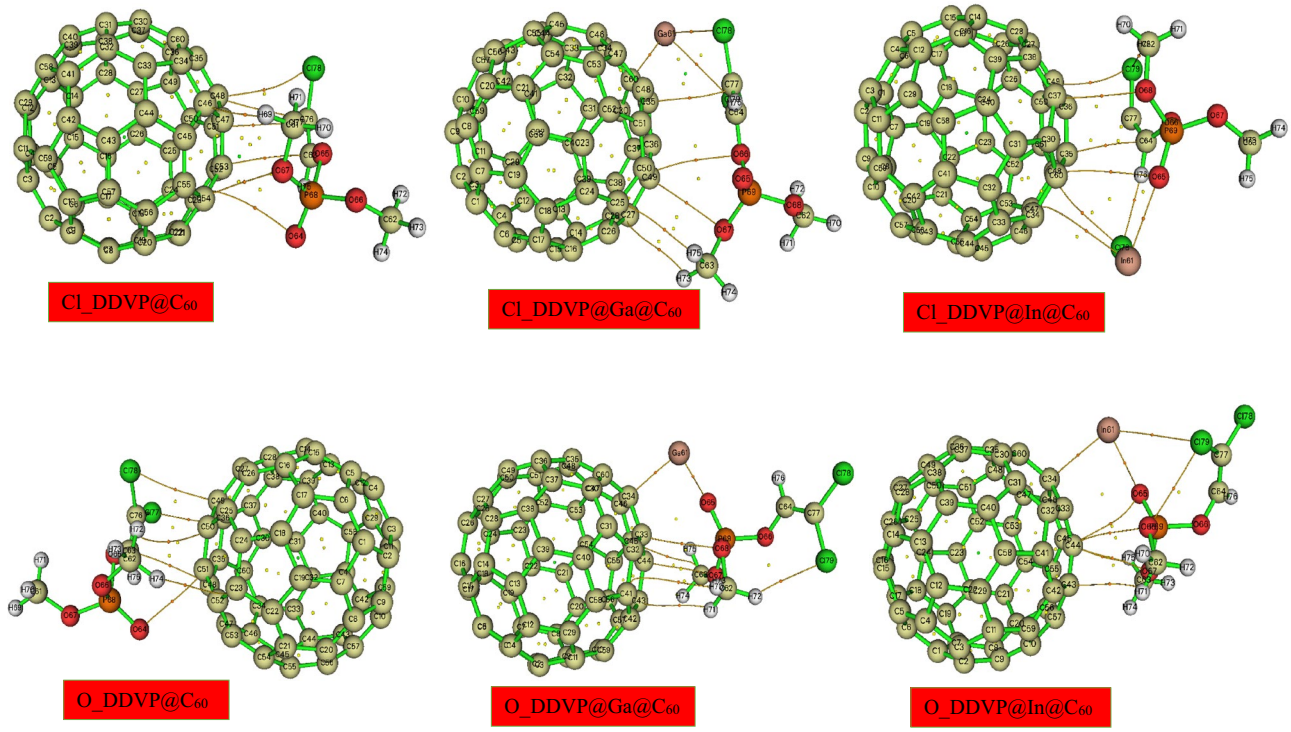

Figure 5. The QTAIM molecular graphs for all studied complexes studied at the Cl and O sites of DDVP. The bond critical points (BCPs) interactions represented with green lines while the brown lines indicate the interactions.

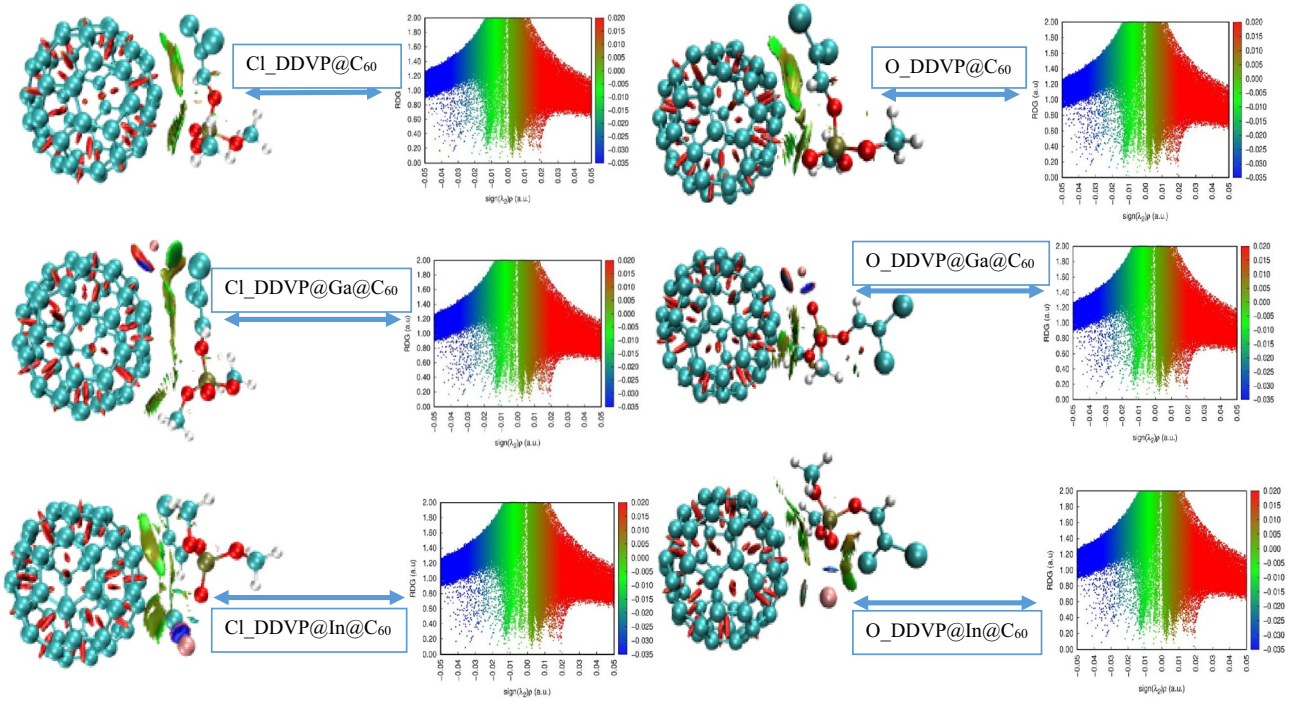

Figure 6. The 2D and 3D Isosurface maps of the Non-covalent interaction analysis performed for the various interactions at both sites of adsorption to characterize the nature of bonds present using the VMD software.

$$\sigma = AT^{3/2}e^{(-Eg/2kT)} \tag{7}$$

Another parameter that is very crucial in developing a biosensor is the work function. The work function (ϕ) is the minimum amount of energy required to remove the weakest bound electron from the fermi energy level in the solid surface to a vacuum point. It is directly proportional to the fermi energy from their mathematical relationship where the proportionality constant is − 1. It is also a suitable indicator that provides a better understanding of the reactivity and sensitivity of nanostructures towards adsorption of different molecules[70,71]. From the Table 5, the work function values ranged from − 3.279 to − 8.191 eV. High work function values entail high fermi energy values and vice versa. The results in Table 5 also shows that the surface has lower work function value (− 4.816 eV) when decorated on the Cl site of the compound (DDVP) compared to when decorated with O site, where its value is − 5.510 eV. This may be due to the difference in their electronegativity, where O is more electronegative than Cl. However, work function values of the Cl decorated compound became slightly higher than those of O decorated compound when the both were doped with Ga and In. The values are (− 3.891 eV for Ga doped and − 4.816 eV for Indium In doped) also (− 3.374 eV for Ga doped and − 3.279 eV for In doped) for Cl and O decorated compound respectively. The work function can be expressed through Eq. (8)

$$\Phi = V_{el\,(+\infty)} - E_{FL} \tag{8}$$

Systems	INTER. SYST	E_{FL} (eV)	ϕ (eV)	Q_t (eV)
C_{60}	–	8.191	− 8.191	–
DDVP	–	3.524	− 3.524	–
Ga@C_{60}	–	4.122	− 4.122	–
In@C_{60}	–	3.959	− 3.959	–
Cl_DDVP@C_{60}	C_{53}–Cl_{78}	4.816	− 4.816	− 0.0437
Cl_DDVP@Ga@C_{60}	Ga_{61}–Cl_{78}	3.891	− 3.891	0.3121
Cl_DDVP@In@C_{60}	In_{61}–Cl_{78}	4.816	− 4.816	1.3796
O_DDVP@C_{60}	C_{51}–O_{64}	5.510	− 5.510	1.0239
O_DDVP@Ga@C_{60}	Ga_{61}–O_{65}	3.374	− 3.374	1.9417
O_DDVP@In@C_{60}	In_{61}–O_{65}	3.279	− 3.279	1.2056

Table 5. Calculated sensing mechanism parameters of studied systems employing the DFT/B3LYP-GD3BJ/def2svp level of theory.

where $V_{el(+\infty)}$ is the vacuum electrostatic potential energy (which is assumed to be ≈ 0), E_{FL} is the fermi energy level. Based on the assumption that $V_{el(+\infty)} \approx 0$, therefore, $\Phi = -E_{FL}$. This implies that work function is directly proportional to the negative value of the fermi energy, which means that a change in the fermi energy level equates to a change in the work function as shown in Table 5. Like the work function, the fermi energy values ranged from 3.279 to 8.191 eV. The results in Table 5 also shows that the surface has lower work function value (4.816 eV) when decorated with the Cl atom of the compound (DDVP) compared to when decorated with O atom, where its value is 5.510 eV. This may be due to the difference in their electronegativity, where O is more electronegative than Cl. However, work function values of the Cl decorated compound became slightly higher than those of O decorated compound when the both were doped with Ga and In. The values are (3.891 eV for Ga doped and 4.816 eV for In doped) and (3.374 eV for Ga doped and 3.279 eV for In doped) for Cl and O decorated compound respectively.

The charge transfer (Q_t) is the difference between the charge on the adsorbent (i.e. the nanostructure) and the charge on the isolated compound. A positive value of the charge transfer indicates that there is transfer of charges from the nanostructure (adsorbent) to the compound, while a negative value of the charge transfer indicates that there is transfer of charges from the compound to the nanostructure and is related mathematically using Eq. (9)[52].

$$Q_t = Q_{ads} - Q_{isolated} \tag{9}$$

From the table above, only C_{53}–Cl_{78} interaction gave a negative value of − 0.0437 eV, indicating that charge transfer is from the compound (DDVP) to the nanostructure (adsorbent). This might be due to the fact that the nanostructure was not doped with any metallic or metalloid atom like the others where the nanostructure was decoration with gallium (Ga) and indium (In) before interaction with the compound, and they gave positive values of charge transfer, indicating that charges were transferred from the Ga and In decoration nanostructured to the compound. Also, Ga and In decoration nanostructured interacted with the compound at the O-atom gave higher positive Q_t values than those interacted with the compound at the Cl-atom. Ga_{61}–O_{65} and In_{61}–O_{65} interaction values are 1.9417 eV and 1.2056 eV respectively, while Ga_{61}–Cl_{78} and In_{61}–Cl_{78} interaction values are 0.3121 eV and 1.3796 eV respectively. This might be as a result of the higher electronegativity of oxygen compared to that of chlorine. The intramolecular interactions of NBOs within the structure might give rise to the intramolecular charge transfer which can affect the stability of the system. Systems that did not involve interaction between the nanostructure and the compound do not have Q_t values as shown in the Table 5. Furthermore, biological binding events and bio conductivity of an electrochemical biosensor material is dependent on changes in its absolute temperature which emanate from a thermally activated process causing changes in resistance, conductance, or capacitance of the biosensor surface. The process is often described by the Arrhenius expression as seen in Eq. (10).

$$K = Ae^{-Ea/RT} \tag{10}$$

Molecular adsorption analysis. Using first principles theoretical approach, the adsorption energy was calculated for sensing in this study using the DFT/B3LYP/def2SVP level of theory for the adsorption of the organophosphate (Dichlorovos) using Gallium (Ga) and Indium (In) decorated fullerene surfaces as the sensor material. The adsorbent material $X@C_{60}$ (X = Ga,In) was interacted with the adsorbate at its chlorine (Cl) and oxygen (O) atom sites, this was done on the bid to determine the best adsorption site for sensing and delivering of the DDVP molecule as an insecticide with minimal or no side effect on human health. Scholarly reported studies and keen literature review showed that strong adsorption energy (E_{ads}) exist when negative (exothermic) calculated E_{ads} value is obtained, which means that the adsorption process is favored (chemisorption). While on the other hand, a positive Eads value suggests a weak adsorption condition which entails that the process is endothermic (physisorption) and may require catalyst activities to enhance the adsorption process[67]. The bio recognition of a substrate or absorbent material by a adsorbate biomolecule is very crucial to take into consideration in designing a sensor material. Using the fullerene material which is highly applicative in sensor designs to sense and trap numerous biomolecules for solving general human conditions, we seize their advantages by enhancing its action with Ga and In metals to promote the interactions, reactivity, improve needed catalytic step and their structural alterations by further adsorption on two sites using the mathematical expression in Eq. (11)[52], while obtained results are recorded on Table 6.

SYSTEMS	$E_{Complex}$ (hartree)	$E_{Surface}$ (hartree)	E_{DDVP} (hartree)	E_{Ads}(kJ/mol)
Cl_DDVP@C_{60}	− 4003.524777	− 2284.851006	− 1718.651726	− 57.894
Cl_DDVP@Ga@C_{60}	− 5928.192894	− 4209.511416	− 1718.651726	− 78.107
Cl_DDVP@In@C_{60}	− 4193.765921	− 2475.076142	− 1718.651726	− 99.901
O_DDVP@C_{60}	− 4003.523450	− 2284.851006	− 1718.651726	− 54.400
O_DDVP@Ga@C_{60}	− 5928.206584	− 4209.511416	− 1718.651726	− 114.060
O_DDVP@In@C_{60}	− 4193.771312	− 2475.076142	− 1718.651726	− 114.056

Table 6. Calculated and tabulated adsorption energies of all studied complexes using the optimized structures obtained from the B3LYP-GD3BJ/ def2svp level of theory.

$$E_{ads} = E_{complex} - (E_{surface} + E_{DDVP}) \quad (11)$$

According to the results as depicted on Table 6, the adsorption energy observed for the Cl site of interaction were − 57.894 kJ/mol, − 78.107 kJ/mol, and − 99.901 kJ/mol for Cl_DDVP@C_{60}, Cl_DDVP@Ga@C_{60} and Cl_DDVP@In@C_{60} interactions respectively while at the O site of adsorption, the E_{ads} values were seen as − 54.400 kJ/mol, − 114.060 kJ/mol and − 114.056 kJ/mol corresponding to O_DDVP@C_{60}, O_DDVP@Ga@C_{60} and O_DDVP@In@C_{60} respectively. The adsorption energy analysis herein shows the chemisorption strength between the individual surfaces and their corresponding interactions with the DDVP molecule at their Cl and O site of adsorption and it is crystal clear that the adsorption energy is greater at the O adsorption site compared to the Cl site which is not a favorable adsorption site as can be seen in the thermodynamics analysis of the interactions. This high reactivity and conductivity at the oxygen site of DDVP could be due to the metallic oxides (bond) formed between oxygen (O) and group 13 elements which include Ga and In metals. The adsorption energy results suggest high reactivity, selectivity and conductivity between the adsorbent and adsorbate molecules, thereby displaying them as promising sensor materials for sensing DDVP and adsorption strength can be ranked as follows O_DDVP@Ga@C_{60} > O_DDVP@In@C_{60} > Cl_DDVP@In@C_{60} > Cl_DDVP@Ga@C_{60} > Cl_DDVP@C_{60} > O_DDVP@C_{60} according to the E_{ads} analysis.

Molecular thermodynamics analysis. Thermodynamic properties involving energy of the reactions, work and heat transfer from the adsorbent pristine and metal (Ga, In) doped surfaces to the DDVP adsorbate, were studied by applying thermodynamic parameters like the entropy (ΔS), enthalpy (ΔH) and Gibbs free (ΔG) energy to further confirm the reactivity, conductivity and adsorption of the adsorbate on the different surfaces on both sites of adsorption done at the DFT/B3LYP/def2SVP level of theory. Entropy is simply the degree of disorderliness of a system. The enthalpy is a useful parameter for ascertaining stability of systems, it is the total energy of the system at constant pressure and it is given as ΔH = E + PV. In DFT calculations, the enthalpy is obtained from the subtraction of the reacting systems from the product. Scholarly reported research had previously reported that when ΔH > 0 the reaction is endothermic and is not chemically favored whereas ΔH < 0 is exothermic in nature and suggest favorable condition of the reactants forming products and was calculated using the mathematical expression in Eqs. (12) and (13)[52].

$$\Delta H^0(298\,K) = \Sigma \text{ product } \Delta_f H^0 \text{ prod}(298\,k) - \Sigma \text{ reactant } \Delta_f H^0 \text{ react}(298\,k) \quad (12)$$

$$\Delta_f H^0(298\,k) = \Sigma(E_0 + H_{corr}) \text{ product} - \Sigma(E_0 + H_{corr}) \text{ reactants} \quad (13)$$

where ε_0 represents electronic energy of the reactant and product and H_{corr} is the sum of electronic energy and thermal correction to H).

The standard free energy (ΔG) was also studied herein. The free energy can be seen as the measure of the energy available to do work. It gives us insights on whether a system is spontaneous or non-spontaneous. It is the change in the enthalpy (ΔH) minus the absolute product of the change in entropy (ΔS) and the temperature (K) of the system and was calculated for these studies using Eq. (14)[52].

$$\Delta_f G^0(298) = \sum (\varepsilon_0 + G_{corr}) \text{ product} - \sum (\varepsilon_0 + G_{corr}) \text{ reactants} \quad (14)$$

Evidence from previous researchers shows that for a reaction to be spontaneous the standard Gibbs free ΔrG^0 (298 K) must be negative, while positive standard Gibbs free ΔrG^0 (298 k) shows non spontaneity of reaction or process. The thermodynamic results for these studies are recorded on Table 7 for the calculated values and Table S1 of the supporting information for the GuassView obtained result respectively. According to the obtained results, the standard enthalpy (ΔrH^0) and standard Gibbs free (ΔG^0) observed for the interactions at the Cl adsorption site were − 52.510 kJ/mol and − 5.251 kJ/mol, − 1614.683 kJ/mol and − 1703.950 kJ/mol, − 2885.425 kJ/mol and − 2969.441 kJ/mol corresponding to Cl_DDVP@C_{60}, Cl_DDVP@Ga@C_{60} and Cl_DDVP@In@C_{60} respectively. This result shows that the systems or interactions are highly unstable which is evident on the very high ΔH value except for the bare interaction (Cl_DDVP@C_{60}) which is considerably stable at the site of adsorption. Also, in the ΔG values observed herein, the values were also too high showing the unfavorable adsorption occurring between the adsorbate and adsorbent surfaces. Conversely, on the O adsorption site, the

Systems	ΔS (kJ/mol)	ΔrH^0 (kJ/mol)	ΔrG^0 (kJ/mol)
Cl_DDVP@C_{60}	219.178	− 52.510	− 5.251
Cl_DDVP@Ga@C_{60}	202.351	− 1614.683	− 1703.950
Cl_DDVP@In@C_{60}	209.121	− 2885.425	− 2969.441
O_DDVP@C_{60}	219.600	− 49.885	− 2.626
O_DDVP@Ga@C_{60}	194.868	− 632.746	− 729.889
O_DDVP@In@C_{60}	192.896	− 630.120	− 719.387

Table 7. Calculated thermodynamic properties including the enthalpy (ΔH) and Gibbs free energy (ΔG) calculated for all interactions at the B3LYP-GD3BJ/ def2svp level of theory.

standard enthalpy and free energy observed were − 49.885 kJ/mol and − 2.626 kJ/mol, − 632.746 kJ/mol and − 729.889 kJ/mol, − 630.220 kJ/mol and − 719.387 kJ/mol for O_DDVP@C_{60}, O_DDVP@Ga@C_{60} and O_DDVP@In@C_{60} systems respectively. The ΔH and ΔG obtained at this site of adsorption is considerably stable and the reaction is spontaneous and was in the order O_DDVP@Ga@C_{60} > O_DDVP@In@C_{60} > O_DDVP@C_{60}. This result presents that the organophosphate molecule (DDVP) can be highly detected by the metal decorated surfaces adsorbed on the oxygen (O) site of the biomolecule.

Conclusions

Herein, first-principles theoretical calculations utilizing the geometry optimization at the Becke three parameter Lee–Yang–Parr exchange-functional (B3LYP) together with Def2svp basis set, were employed to determine the efficacy of Dichlorovos (DDVP) an organophosphate molecule on C_{60} fullerene nanocage and its doped metal surfaces through the chlorine (Cl) and oxygen (O) sites of the molecule involving Cl_DDVP@C_{60}, Cl_DDVP@C_{60} and Cl_DDVP@C_{60} at the Cl site, while O_DDVP@C_{60}, O_DDVP@Ga@C_{60} and O_DDVP@In@C_{60} on the O site. The fullerene surfaces are acting as biosensor for the effective adsorption and trapping of DDVP (which is widely used as an insecticide) in order to enhance the control and management of household pests and other disease-causing pest. Exploring different theoretical approaches, the geometric structural analysis on the chlorine and oxygen adsorption site of DDVP suggested that the compounds are reactive on adsorption especially the metal doped surfaces which showed an increased reactivity on adsorption of DDVP which are justified by the increase in bonds which suggest their structural adaptation with an external reacting specie. we observed from the frontier molecular orbital (FMO) analysis that there was a rise in reactivity of the fullerene semiconductor material when the metals were introduced on the cage as well as when DDVP was adsorbed on the surfaces on both the Cl and O site of adsorption which led to the small band gap observed as seen on Table 2 except for Cl_DDVP@In@C_{60}. The density of state analysis showed the most contributive atom fragments in all the interactions. The natural bond orbital analysis showed the stabilization energy of all the different interactions and the result showed that there was higher electron stability in terms of electron transfer from the donor to acceptor orbital in the O adsorption site of interactions. The topological analysis involving the Quantum theory of atoms in molecules (QTAIM) and the Non covalent interaction (NCI) shows that majorly non covalent interaction exists between the adsorbate and adsorbent and was further confirmed in the NCI reduced gradients 2D and 3D surface plot and was observed that the weak interactions are more on the Cl site of DDVP interactions. The sensor mechanisms were used to elucidate the electronic charge transfer, reactivity and conductivity of the different interactions. The adsorption energy analysis shows that the interactions of Cl_DDVP@C_{60}, Cl_DDVP@Ga@C_{60} and Cl_DDVP@In@C_{60} are not favorable and weak in nature and hence exhibits a non-stable adsorption. Meanwhile adsorption energies at the O adsorption site shows a considerably stable adsorptions and hence was exothermic meaning that the reaction between the reactants would favor the formation of product, this could be due to the metallic bonds form between oxygen and transition metals. The thermodynamic studies further confirmed the adsorption studies which show the spontaneous reaction in O_DDVP@C_{60}, O_DDVP@Ga@C_{60}, and O_DDVP@In@C_{60} as to when compared to the interactions on the Cl site where very high energies are observed showing unfavorable adsorptions. Meanwhile, the adsorption of DDVP through its O specific site on the adsorbent were observed in the order O_DDVP@Ga@C_{60} > O_DDVP@In@C_{60} > O_DDVP@C_{60}.

Data availability

All data are contained within the manuscript and electronic supporting information (ESI).

Received: 27 April 2023; Accepted: 25 June 2023
Published online: 28 June 2023

References

1. Dhananjayan, V., Jayakumar, S., & Ravichandran, B. Conventional methods of pesticide application in agricultural field and fate of the pesticides in the environment and human health. *Control. Release Pestic. Sustain. Agric.* 1–39 (2020).
2. Gupta, R. C. *Classification and Uses of Organophosphate and Carbamates. Toxicology of Organophosphate and Carbamate Compounds* 5–24 (Academic Press, 2006).
3. National Centre for Biotechnology Information. PubChem compound summary for CID 3039, Dichlorvos (accessed 10 January 2023), https://pubchem.ncbi.nlm.nih.gov/compound/Dichlorvos (2023).
4. Owoeye, O. *et al.* Toxicological changes in liver and lungs of rats exposed to dichlorvos before and after vitamin supplementation. *Eur. J Anat.* **16**(3), 190–198 (2012).
5. Okoroiwu, H. U. & Iwara, I. A. Dichlorvos toxicity: a public health perspective. *Interdiscip. Toxicol.* **11**(2), 129 (2018).
6. USEPA: United States Environmental Protection Agency. *Dichlorvos TEACH Chemical Summary U.S EPA, Toxicity and Exposure Assessment for Children*, 1–13 (2007)
7. Budavari, S. *Merck Index: An Encyclopedia of Chemicals, Drugs and Biologicals* 11th edn. (Merck and Company Inc., 1998).
8. Zhang, Y. *et al.* Emerging technologies for degradation of dichlorvos: A review. *Int. J. Environ. Res. Public Health* **18**(11), 5789 (2021).
9. Mulla, S. I. *et al.* Organophosphate pesticides: Impact on environment, toxicity, and their degradation. *Bioremediation Ind. Waste Environ. Saf. Vol. I Ind. Waste Manag.* https://doi.org/10.1007/978-981-13-1891-7_13 (2020).
10. Binukumar, B. K. & Gill, K. D. Cellular and molecular mechanisms of dichlorvos neurotoxicity: cholinergic, noncholinergic, cell signaling, gene expression and therapeutic aspect. *Indian J. Exp. Biol.* **48**, 697–709 (2010).
11. USEPA: United states Environmental Protection Agency. Dichlorvos (DDVP), naled and Trichlorfon: Drinking water assessment for registration review (2020)
12. Grandjean, P. & Landrigan, P. J. Neurobehavioural effects of developmental toxicity. *Lancet Neurol.* **13**, 330–338. https://doi.org/10.1016/S1474-4422(13)70278-3 (2014).
13. Rathod, A. L. & Garg, R. Chlorpyrifos poisoning and its implications in human fatal cases: A forensic perspective with reference to Indian scenario. *J. Forensic Leg. Med.* **47**, 29–34. https://doi.org/10.1016/j.jflm.2017.02.003 (2017).

14. Nasrollahzadeh, M., Sajadi, S. M., Sajjadi, M., Issaabadi, Z. Chapter 1- An introduction to nanotechnology, Vol. 28, 1–27, ISSN 1573-4285 https://www.sciencedirect.com/science/article/pii/B9780128135860000018 (2019).
15. Yang, L. *et al.* C60@C3N4 nanocomposites as quencher for signal-off photoelectrochemical aptasensor with Au nanoparticle decorated perylene tetracarboxylic acid as platform. *Anal. Chim. Acta* **1077**, 281–287. https://doi.org/10.1016/j.aca.2019.05.058 (2019).
16. Keshtkar, S. *et al.* A novel highly sensitive and selective H_2S gas sensor at low temperatures based on SnO_2 quantum dots-C60 nanohybrid: Experimental and theory study. *Talanta* **188**, 531–539. https://doi.org/10.1016/j.talanta.2018.05.099 (2018).
17. Zhang, H. *et al.* Graphene-enabled wearable sensors for healthcare monitoring. *Biosens. Bioelectron.* **197**, 113777. https://doi.org/10.1016/j.bios.2021.113777 (2022).
18. Du, J. H. *et al.* Advances in flexible optoelectronics based on chemical vapour deposition- growth graphene. *Adv. Funct. Mater.* **32**, 2203115. https://doi.org/10.1002/adfm.202203115 (2022).
19. Chaudhary, V. *et al.* Towards hospital -0n-chip supported by 2D MXenes-based 5th generation intelligent biosensors. *Biosens. Bioelectron.* **220**, 114847. https://doi.org/10.1016/j.bios.2022.114847 (2023).
20. Mazari, S. A. *et al.* Nanomaterials: Applications, waste-handling, environmental toxicities, and future challenges–A review. *J. Environ. Chem. Eng.* **9**(2), 105028 (2021).
21. Gounden, D., Nombona, N. & Van Zyl, W. E. Recent advances in phthalocyanines for chemical sensor, non-linear optics (NLO) and energy storage applications. *Coord. Chem. Rev.* **420**, 213359 (2020).
22. Liu, Z., Zhang, X., Yan, X., Chen, Y. & Tian, J. Nonlinear optical properties of graphene-based materials. *Chin. Sci. Bull.* **57**, 2971–2982 (2012).
23. Sadeghi, M. *et al.* Dichlorosilane adsorption on the Al, Ga, and Zn-doped fullerenes. *Monatsh Chem.* **153**, 427–434. https://doi.org/10.1007/s00706-022-02926-8 (2022).
24. Moses Abraham, B. Adsorption of cyanogen halides (X-CN; X = F, Cl and Br) on pristine and Fe, Mn doped C60: A highly potential gas sensor. *Mater. Today Commun.* **26**, 101901. https://doi.org/10.1016/j.mtcomm.2020.101901 (2021).
25. Muz, S. & Kurban, M. A first principles evaluation on the interaction of 1,3,4-oxadiazole with pristine and B-, Al- Ga-doped C60 fullerenes. *J. Mol. Liq.* **335**, 116181. https://doi.org/10.1016/j.molliq.2021.116181 (2021).
26. Parlak, C., Alver, Ö. & Bağlayan, Ö. Quantum mechanical simulation of molnupiravir drug interaction with si-doped C60 fullerene. *Comput. Theor. Chem.* **1202**, 113336. https://doi.org/10.1016/j.comptc.2021.11336 (2021).
27. SkenerMuz, A. Enhanced adsorption of fluoroquinolone antibiotic on the surface of the Mg-, Ca-, Fe-, and Zn- doped C60 fullerenes: DFT and TD-DFT approach. *Mater. Today Commun.* **31**, 103798. https://doi.org/10.1016/j.mtcomm.2022.103798 (2022).
28. Jiang, Z. *et al.* Adsorption of sulfonamides on polyamide microplastics in an aqueous solution: Behavior, structural effects, and its mechanism. *Chem. Eng. J.* **454**, 140452 (2023).
29. Zhao, Z. Y. *et al.* Environmental risk of multi-year polythene film mulching and its green solution in arid irrigation region. *J. Hazard. Mater.* **435**, 128981 (2022).
30. Chen, D. *et al.* A general linear free energy relationship for predicting partition coefficients of neutral organic compounds. *Chemosphere* **247**, 125869 (2020).
31. Zhao, Y., Li, Q., Cui, Q. & Ni, S. Q. Nitrogen recovery through fermentative dissimilatory nitrate reduction to ammonium (DNRA): Carbon source comparison and metabolic pathway. *Chem. Eng. J.* **441**, 135938 (2022).
32. Liu, W. *et al.* Effective extraction of Cr (VI) from hazardous gypsum sludge via controlling the phase transformation and chromium species. *Environ. Sci. Technol.* **52**(22), 13336–13342 (2018).
33. Zhang, T. *et al.* Improving the humification and phosphorus flow during swine manure composting: A trial for enhancing the beneficial applications of hazardous biowastes. *J. Hazard. Mater.* **425**, 127906 (2022).
34. Frisch, M. E., Trucks, G. W., Schlegel, H. B., Scuseria, G. E., Robb, M. A., Cheeseman, J. R., & Fox, D. J. *et al* Gaussian 16 (2016).
35. Weinhold, F., & Glendening, E. D. NBO 5.0 program manual: Natural bond orbital analysis programs. *Theor. Chem. Inst. Dep. Chem. Univ. Wis. Madison WI 53706* (2001).
36. Lu, T. & Chen, F. Multiwfn: A multifunctional wavefunction analyzer. *J. Comput. Chem.* **33**(5), 580–592 (2012).
37. Humphrey, W., Dalke, A. & Schulten, K. VMD: Visual molecular dynamics. *J. Mol. Graph.* **14**(1), 33–38 (1996).
38. Yudanov, I. V., Genest, A., Schauermann, S., Freund, H. J. & Rösch, N. Size dependence of the adsorption energy of CO on metal nanoparticles: A DFT search for the minimum value. *Nano Lett.* **12**(4), 2134–2139 (2012).
39. Popovic, M. Thermodynamic properties of microorganisms: determination and analysis of enthalpy, entropy, and Gibbs free energy of biomass, cells and colonies of 32 microorganism species. *Heliyon* **5**(6), e01950 (2019).
40. Benjamin, I. *et al.* Antimalarial potential of naphthalene-sulfonic acid derivatives: Molecular electronic properties, vibrational assignments, and in-silico molecular docking studies. *J. Mol. Struct.* **1264**, 133298 (2022).
41. Gber, T. E. *et al.* Heteroatoms (Si, B, N, and P) doped 2D monolayer MoS_2 for NH_3 gas detection. *RSC Adv.* **12**(40), 25992–26010 (2022).
42. Edet, H. O. *et al.* Hydrogen storage capacity of C12X12 (X = N, P, and Si). *Chem. Phys. Impact* **5**, 100107 (2022).
43. Louis, H. *et al.* Probing the reactions of thiourea (CH4N2S) with metals (X= Au, Hf, Hg, Ir, Os, W, Pt, and Re) anchored on fullerene surfaces (C59X). *ACS Omega* **7**(39), 35118–35135 (2022).
44. Agwamba, E. C., Louis, H., Benjamin, I., Apebende, C. G., Unimuke, T. O., Edet, H. O., & Adeyinka, A. S. *et al* (E)-2-((3-nitrophenyl) diazenyl)-3-oxo-3-phenylpropanal: experimental, DFT studies, and molecular docking investigations. *Chem. Afr.* 1–17 (2022).
45. Benjamin, I. *et al.* Modelling of aminothiophene-carbonitrile derivatives as potential drug candidates for hepatitis B and C. *Iran. J. Sci. Technol. Trans. A Sci.* **46**(5), 1399–1412 (2022).
46. Inah, B. E., Louis, H., Benjamin, I., Unimuke, T. O., & Adeyinka, A. S. Computational study on the interactions of functionalized C24NC (NC= C, –OH, –NH2, –COOH, and B) with chloroethylphenylbutanoic acid. *Can. J. Chem.* (2022).
47. Ntui, T. N., Oyo-Ita, E. E., Agwupuye, J. A., Benjamin, I., Eko, I. J., Ubana, E. I., & Imojara, A. *et al* Synthesis, spectroscopic, DFT study, and molecular modeling of thiophene-carbonitrile against enoyl-ACP reductase receptor. *Chem. Afr.* 1–22 (2022).
48. Edet, H. O. *et al.* Heteroatoms (B, N, S) doped quantum dots as potential drug delivery system for isoniazid: Insight from DFT, NCI, and QTAIM. *Heliyon* **9**(1), e12599 (2023).
49. Ikeuba, A. I. *et al.* Green approach towards corrosion inhibition of mild steel during acid pickling using chlorpheniramine: Experimental and DFT study. *Chem. Afr.* **6**(2), 983–997 (2023).
50. Chukwuemeka, K. *et al.* Therapeutic potential of B12N12-X (X = Au, Os, and Pt) nanostructured as effective fluorouracil (5Fu) drug delivery materials. *ACS Appl. Bio Mater.* **6**(3), 1146–1160 (2023).
51. Apebende, C. G. *et al.* Density functional theory (DFT) computation of pristine and metal-doped MC59 (M = Au, Hf, Hg, Ir) fullerenes as nitrosourea drug delivery systems. *Mater. Sci. Semicond. Process.* **158**, 107362 (2023).
52. Benjamin, I. *et al.* Transition metal-decorated B12N12–X (X= Au, Cu, Ni, Os, Pt, and Zn) nanoclusters as biosensors for carboplatin. *ACS Omega* **8**(11), 10006–10021 (2023).
53. Agwamba, E. C. *et al.* Synthesis, characterization, DFT studies, and molecular modeling of azo dye derivatives as potential candidate for trypanosomiasis treatment. *Chem. Phys. Impact* **4**, 100076 (2022).
54. Makhlouf, J. *et al.* Single crystal investigations, spectral analysis, DFT studies, antioxidants, and molecular docking investigations of novel hexaisothiocyanato chromate complex. *J. Mol. Struct.* **1272**, 134223 (2023).

55. Afahanam, L. E. *et al.* Heteroatom (B, N, P, and S)-doped cyclodextrin as a hydroxyurea (HU) drug nanocarrier: A computational approach. *ACS Omega* **8**(11), 9861–9872 (2023).
56. Eno, E. A. *et al.* Experimental and computational modeling of the biological activity of benzaldehyde sulphur trioxide as a potential drug for the treatment of Alzheimer disease. *J. Indian Chem. Soc.* **99**(7), 100532 (2022).
57. Asogwa, F. C. *et al.* Structural benchmarking, density functional theory simulation, spectroscopic investigation and molecular docking of N-(1H-pyrrol-2-yl) methylene)-4-methylaniline as castration-resistant prostate cancer chemotherapeutic agent. *Chem. Phys. Impact* **5**, 100091 (2022).
58. Agwamba, E. C. *et al.* Antitubercolusic potential of amino-(formylphenyl) diazenyl-hydroxyl and nitro-substituted naphthalene-sulfonic acid derivatives: Experimental and theoretical investigations. *Chem. Afr.* **5**(5), 1451–1467 (2022).
59. Louis, H. *et al.* Systematic exo-endo encapsulation of hydroxyurea (HU) by Cu, Ag, and Au-doped gallium nitride nanotubes (GaNNT) for smart therapeutic delivery. *Comput. Biol. Med.* **161**, 106934 (2023).
60. Louis, H. *et al.* Functionalized (-HCO,-OH,-NH2) Iridium-doped Graphene (Ir@ Gp) nanomaterials for enhanced delivery of Piroxicam: Insights from quantum chemical calculations. *J. Mol. Liq.* **383**, 122068 (2023).
61. Nwagu, A. D. *et al.* Computational study on nickel doped encapsulated Mg, K, Ca on pristine C24 nanocage for gas sensing applications. *Mater. Sci. Semicond. Process.* **157**, 107334 (2023).
62. Agwamba, E. C., Mathias, G. E., Louis, H., Ikenyirimba, O. J., Unimuke, T. O., Ahuekwe, E. F., & Adeyinka, A. S. *et al* Single metal-doped silicon (Si59X; X = Nb, Mo, Y, Zr) nanostructured as nanosensors for N-Nitrosodimethylamine (NDMA) pollutant: Intuition from computational study. *Mater. Today Commun.* 106173 (2023).
63. Bader, R. F. Atoms in molecules. *Acc. Chem. Res.* **18**(1), 9–15 (1985).
64. Louis, H. *et al.* Sensor behavior of transition-metals (X = Ag, Au, Pd, and Pt) doped Zn11-X-O12 nanostructured materials for the detection of serotonin. *Mater. Today Commun.* **34**, 105048 (2023).
65. Agwamba, E. C. *et al.* Adsorption mechanism of AsH3 pollutant on metal-functionalized coronene C24H12-X (X = Mg, Al, K) quantum dots. *Chem. Phys. Impact* **6**, 100224 (2023).
66. Agwamba, E. C. *et al.* Investigation of the site-specific binding interactions and sensitivity of ochratoxin with aluminum nitride (Al12N12) nanoclusters. An intuition from quantum chemical calculations. *Chem. Phys. Impact* **6**, 100221 (2023).
67. Louis, H. *et al.* Modelling of tungsten (C59W), osmium (C59Os), and platinum (C59Pt) doped fullerenes for drug delivery of biguanides (BNG) and metformin (MET): DFT perspective. *ChemistrySelect* **8**(1), e202203298 (2023).
68. Louis, H., Amodu, I. O., Eno, E. A., Benjamin, I., Gber, T. E., Unimuke, T. O., & Adeyinka, A. S. *et al* Modeling the Interactionof F-gases on ruthenium-doped boron nitridenanotube. *Chem. Afr.* 1–19 (2023).
69. Abad, N. *et al.* Synthesis, non-covalent interactions and chemical reactivity of 1-pentyl-3-phenylquinoxalin-2 (1H)-one—Structural and computational studies. *J. Mol. Struct.* **1286**, 135622 (2023).
70. Kamal, S., Khalid, M., Khan, M. S. & Shahid, M. Metal organic frameworks and their composites as effective tools for sensing environmental hazards: An up-to-date tale of mechanism, current trends and future prospects. *Coord. Chem. Rev.* **474**, 214859 (2023).
71. Zhang, Y. *et al.* A review of wearable carbon-based sensors for strain detection: Fabrication methods, properties, and mechanisms. *Text. Res. J.* **93**, 2918–2940 (2023).

Acknowledgements
The authors would like to acknowledge the Centre for high performance computing (CHPC), South Africa for providing computational resources for this research project.

Author contributions
H.L.: Project conceptualization, design, resources and supervision. M.A.A.: Writing, results extraction, analysis and manuscript first draft: G.A.O. and I.B.: Visualization, analysis and writing. M.U.A. and O.I.B.: Analysis, reviewing, writing, and editing. S.A.A.: Writing, review, and editing. A.S.A.: Resources, writing, and editing.

Funding
This research was not funded by any Governmental or Non-governmental agency.

Competing interests
The authors declare no competing interests.

Additional information
Supplementary Information The online version contains supplementary material available at https://doi.org/10.1038/s41598-023-37650-8.

Correspondence and requests for materials should be addressed to H.L. or I.B.

Reprints and permissions information is available at www.nature.com/reprints.

Publisher's note Springer Nature remains neutral with regard to jurisdictional claims in published maps and institutional affiliations.